Applied Catalysis B: Environmental 185 (2016) 22–30

Contents lists available at ScienceDirect

Applied Catalysis B: Environmental

journal homepage: www.elsevier.com/locate/apcatb

Insights into the mechanism of heterogeneous activation of persulfate with a clay/iron-based catalyst under visible LED light irradiation

Yaowen Gao[a,b], Zhuoyue Zhang[a], Simiao Li[a], Jin Liu[a], Linyu Yao[a], Yixi Li[a], Hui Zhang[a,b,*]

[a] Department of Environmental Engineering, Wuhan University, Wuhan 430079, China
[b] Shenzhen Research Institute of Wuhan University, Shenzhen 518057, China

ARTICLE INFO

Article history:
Received 20 September 2015
Received in revised form
22 November 2015
Accepted 1 December 2015
Available online 2 December 2015

Keywords:
Kaolinite
Visible LED light
Persulfate
Photocatalytic degradation
Near-neutral pH

ABSTRACT

Activation of persulfate (PS) by ultraviolet (UV) light or metal catalysts has been extensively studied, however, little is known about the activation of persulfate by clay-based catalysts in the presence of visible light-emitting diode (LED) irradiation. Herein, a novel kaolinite-supported iron oxide (K-Fe)/PS/Vis process for the degradation of Rhodamine B (RhB) from aqueous solution is reported. It was found that although persulfate can degrade RhB via a non-radical reaction, the excited RhB molecule (RhB^*) and the Fe(II) species formed on the catalyst surface can effectively activate persulfate to generate radicals which degrade RhB under visible light irradiation. On the basis of quenching experiments and electron paramagnetic resonance (EPR) studies, it is suggested that the free radicals produced from persulfate coupled with the surface-adsorbed radicals formed on the catalyst were responsible for the degradation of the dye via RhB^*. Moreover, the K-Fe catalyst showed excellent reusability and stability with a low level of iron leaching. The findings of this work demonstrate a new pathway for activation of persulfate, which could effectively degrade organic pollutants and also provide some new insights into persulfate remediation of contaminated water.

1. Introduction

In recent years, advanced oxidation processes (AOPs) have been the subject of increasing attention, as shown by the large body of fundamental and applied research work [1–3]. Indeed, AOPs constitute promising, efficient and environmentally-friendly methods to treat water contaminated by recalcitrant organic pollutants involving the generation of highly reactive radicals. Activated persulfate (PS, $S_2O_8^{2-}$) oxidation is regarded as an emerging technology which is gaining importance in water treatment applications, due to PS being relatively cheap, highly soluble in water and stable at ambient temperatures [4–10]. In previous work, the sulfate radical ($SO_4^{\bullet-}$), a strong oxidant with an oxidation–reduction potential of 2.5–3.1 V, was generated through activation of PS by ultraviolet (UV) radiation, heat, quinone, or transition metal catalysis, and the produced $SO_4^{\bullet-}$ can rapidly react with the organic compounds with second-order rate constants in the range of 10^7–10^9 M^{-1} s^{-1} [10].

Although PS can be activated by UV radiation and heat to generate $SO_4^{\bullet-}$, these techniques are restricted in practical applications owing to the requirement of high energy input [11,12]. Recently, transition metals have been utilized to activate PS for the degradation of pollutants in aqueous media [13]. Among the various transition metals, iron (often as dissolved Fe^{2+}) is the most commonly used metallic element for the activation of PS because of its non-toxicity, abundance and effectiveness [5,14–16]. A drawback to the homogeneous reaction involving dissolved ferrous iron is the problem of rapid oxidation and precipitation as ferric iron, which inactivates ferrous iron and incurs additional operation costs for the subsequent removal of iron sludge from the treated water after the reaction.

To address or minimize this problem caused by the presence of residual iron ions in solution and to reduce the recovery cost, the use of heterogeneous catalysis is a promising alternative that could allow conventional operation without the need for soluble iron salts and, hopefully, at near-neutral pH and at ambient temperatures [17]. Various iron-bearing catalysts, such as bulk catalysts containing iron (goethite, hematite and magnetite [18]), can be employed for this process but another approach is the incorporation of iron into various supports and mesoporous silica, zeolite and carbon have been proposed [19–21], but clays offer an interesting alternative source of the required iron.

Using more or less simple techniques, including cationic exchange, pillaring and impregnation processes, the active iron

* Corresponding author at: Department of Environmental Engineering, Wuhan University, Wuhan 430079, China. Fax: +86 27 68778893.
E-mail address: eeng@whu.edu.cn (H. Zhang).

http://dx.doi.org/10.1016/j.apcatb.2015.12.002
0926-3373/

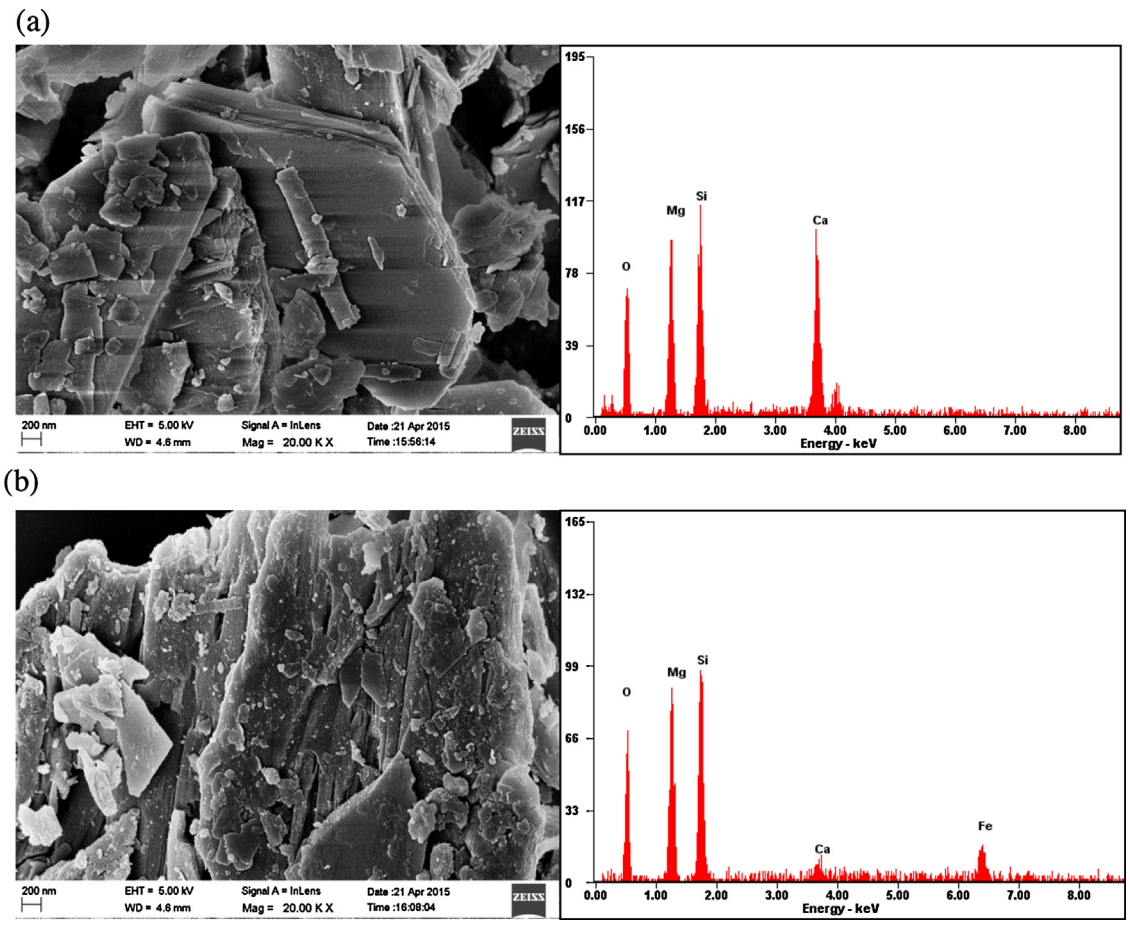

Fig. 1. SEM and the corresponding EDS images of (a) kaolinite and (b) K-Fe.

species can be incorporated into the clay supports. The use of this group of heterogeneous catalysts is particularly beneficial because relatively high mineralization of organic contaminants can be achieved, along with easy separation of the catalysts from the treated wastewater, without causing secondary metal ion pollution. In addition to these advantages, the wide utilization of clays as catalyst support can be attributed to the fact that natural clays are abundant, cheap and the catalyst is simple to prepare [18]. Therefore, clay-based catalysts have been extensively used in the heterogeneous (photo) Fenton-like process with hydrogen peroxide (H_2O_2) as the oxidant [22–26]. Our previous work focused on the photosensitization process of visible light induced heterogeneous Fenton-like degradation of Rhodamine B (RhB) [26] where the dyestuff absorbs visible light and is excited. The subsequent electron transfer from the excited dye molecules to the Fe(III) species on the catalyst provides an impetus for the cycling of Fe(II) and Fe(III) species, thus enhancing the Fenton reactions. However, it is unclear whether the excited dye molecules can react in a similar way with PS to generate the $SO_4^{\bullet-}$ radical. Moreover, to the best of our knowledge, there have been no reports concerning the application of clay-based catalysts on the degradation of organic pollutants by PS under visible light irradiation.

The advancement of solid state semiconductor technology has given great impetus to the development of compact, low cost, and environmentally-friendly light emitting diodes (LEDs) [27]. The visible LEDs are now extensively used in interior and exterior lighting, and they exhibit several merits, such as emitting a relatively narrow spectrum of light, long life span, high spectral purity, uniform illumination, energy efficiency and flexible configuration [28]. LEDs also offer a new alternative to conventional light sources due to their small size and lack of requirement for cooling so they appear ideal candidates for photocatalytic applications in environmental remediation procedures with reduced power consumption, along with greater potential for the design of different types of photoreactors.

Consequently, the primary objectives of this study were: (1) can PS be activated by the excited dye molecules under visible LED light irradiation; (2) can the photocatalytic degradation of RhB be enhanced by the addition of a clay-based catalyst; and (3) what is the underlying mechanism of the photocatalytic degradation process? In the present work, RhB was selected as the model pollutant, since it is representative of an organic dye group which is inexpensive and frequently used in photocatalytic processes [23,24]. Electron paramagnetic resonance (EPR) was employed to identify the radical species generated in the photocatalytic degradation process and a plausible mechanism is proposed.

2. Materials and methods

2.1. Chemicals

Kaolinite provided by the Shanpu Chemical Co., Ltd. (Shanghai, China) was used as the support material. Iron nitrate nonahydrate and sodium persulfate were purchased from the Sinopharm Chemical Reagent Co., Ltd. (Shanghai, China). The spin trapping agent, 5,5-dimethyl-pyrroline-*N*-oxide (DMPO), was purchased from Aladdin, China. The Rhodamine B and phenol employed in the experiments were obtained commercially and used without

further purification. All other reagents were of analytical grade and were prepared in deionized water.

2.2. Experimental setup

The experimental setup and the spectrum of the LED lamps utilized are shown in Figs. S1 and S2, respectively. Specifically, the reactor comprised a 250-mL glass beaker with a 5-m flexible visible light LED strip containing white LED lamps wrapped around it at a distance of 5 cm. The LED lamps emit white light at 455 nm and further broadband Stokes-shift light emitted at roughly 500–600 nm. The average light intensity of LED lamps was 0.47 mW cm^{-2} measured by a digital lux meter (MS 6612, MASTECH, Shenzhen, China). The photo-reactor was covered by a mirror to minimize the penetration of ambient light and the evaporation of water.

2.3. Catalyst preparation and characterization

Kaolinite-supported iron oxide was fabricated according to the method described in the literature [29], but with slight modification (see Supplementary material for details). The morphologies of kaolinite and K-Fe were examined with a field-emission scanning electron microscope (FESEM, Ziess SIGMA) and the elemental composition of samples was characterized by energy-dispersive spectrometry (EDS) using an energy-dispersive X-ray spectrometer (Oxford INCA-400) attached to the SEM instrument. The crystal structure was analyzed by X-ray diffraction (XRD) on a diffractometer (XPert Pro) with Cu Kα radiation of wavelength 1.5406 Å. The X-ray photoelectron spectroscopy (XPS) was carried out on a photoelectron spectrometer (ESCALAB 250Xi, Thermo Fisher) with monochromatic Al Kα radiation. To detect the generation of radical species, electron paramagnetic resonance (EPR) measurements were performed on a spectrometer (JES-FA200, JEOL).

2.4. Experimental procedure and analyses

The degradation of RhB was carried out in a photo-reactor fitted with visible LEDs. In each experiment, an aqueous solution of RhB (200 mL 0.1 mM) was placed in the reactor, followed by the addition of a desired amount of PS and catalyst. The suspension was then magnetically stirred at a constant rate, and the LEDs were switched on. At designated irradiation time intervals aliquots of solution were withdrawn by syringe and immediately filtered (0.45 μm membranes) and then analyzed on a UV–Vis spectrometer (Rayleigh UV-9100) at the maximum wavelength of 554 nm.

The solution pH was measured with a combined glass electrode connected to a Mettler–Toledo FE20 pH meter. The concentration of PS was analyzed via an iodometric titration method and the amount of leached iron ions was determined by spectrophotometry at λ = 510 nm after adding 1,10-phenanthroline to form an iron-phenanthroline complex. The TOC remaining in solution was measured using a Jena multi N/C 3100 TOC analyzer.

3. Results and discussion

3.1. Characterization of the kaolinite-supported iron oxide (K-Fe) catalyst

Fig. 1 presents SEM and the corresponding EDS images of kaolinite and the prepared K-Fe. As can be seen from Fig. 1a, pure kaolinite possesses a plate-like microscopic morphology and a relatively smooth surface, mainly consisting of O, Mg, Si and Ca elements. After introduction of the iron species, the surface of K-Fe became rougher, though, the original structure of kaolinite was maintained during the impregnation process and even after calcination (Fig. 1b). However, some solid particles attached to the surface of the support can be clearly observed, suggesting that an iron species may have been formed, as evidenced by the EDS result shown in Fig. 1b, where the Fe content in K-Fe was found to be 6.91 wt%, while no Fe was detected in the kaolinite.

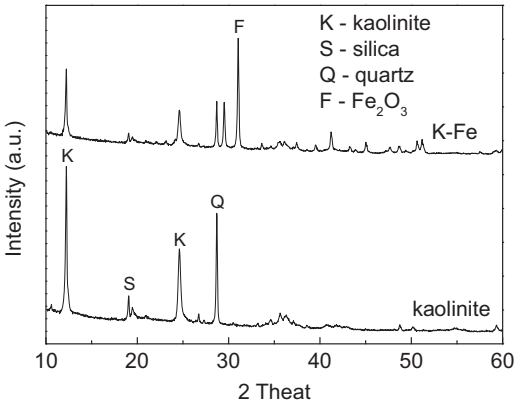

Fig. 2. XRD patterns of kaolinite and K-Fe.

To verify the formation of iron oxide in the K-Fe, the crystal phase of kaolinite before and after processing was analyzed via XRD and the patterns are shown in Fig. 2 and demonstrate that the clay contained kaolinite as the major mineral, with the characteristic reflection at 12.23° and 24.60° [30]. Other peaks associated with impurities such as silica and quartz were also observed in the XRD pattern. In contrast, K-Fe displayed new diffraction peaks at 30.56°, 35.66° and 43.30°, which are attributable to the (1 0 4), (1 1 0) and (2 0 2) reflections of α-Fe_2O_3 (JCPDS, File No. 33-0664) [31], revealing that α-Fe_2O_3 was indeed formed on the surface of K-Fe during preparation, therefore, confirming the observation from the SEM.

In order to further confirm the chemical compositions and the surface states of iron on K-Fe, XPS analysis was carried out and Fig. 3a shows the XPS survey spectrum of K-Fe, indicating the presence of Si, O, Fe, and Mg, which is in accord with the result of the EDS characterization. The high resolution XPS spectra of the Fe 2p region around 720.0 eV (Fig. 3b) and the O1s region around 532.0 eV (Fig. 3c) were further analyzed. As seen in Fig. 3b, the two peaks centered at 711.2 and 724.5 eV can be ascribed to the core levels of Fe 2p3/2 and Fe 2p1/2, respectively and this is consistent with the data previously reported for α-Fe_2O_3 (711.0 and 724.8 eV) [29]. The energy separation between the spin-orbit doublet was 13.3 eV, suggesting the presence of the oxidation state of Fe^{3+} [32]. In addition, a satellite peak located at 719.4 eV further confirmed the existence of Fe^{3+} species on the surface of the K-Fe. The high resolution spectrum of O1s shown in Fig. 3c exhibited three peaks located at 530.3, 531.8 and 532.8 eV after curve fitting, which corresponds to the oxygen species Fe_2O_3, SiO_2 and MgO, respectively [33] and is supportive of the information obtained from SEM, EDS and XRD, indicating that α-Fe_2O_3 had been successfully loaded onto the kaolinite.

3.2. Catalytic activity of K-Fe

The decolorization of RhB was employed to evaluate the catalytic ability of K-Fe, where control experiments were carried out to compare the decolorization efficiencies of various processes at normal pH (pH 5.0) with an initial RhB concentration of 0.1 mM. As shown in Fig. 4, RhB alone is virtually unchanged after 180 min of irradiation with visible light (curve 1), indicating that RhB is quite stable under these conditions. The removal of RhB by adsorption onto K-Fe was not significant without (<10%, curve 2) and with (<14%, curve 3) visible light illumination. When PS was present, it is interesting that approximately 55% of RhB was decolorized after

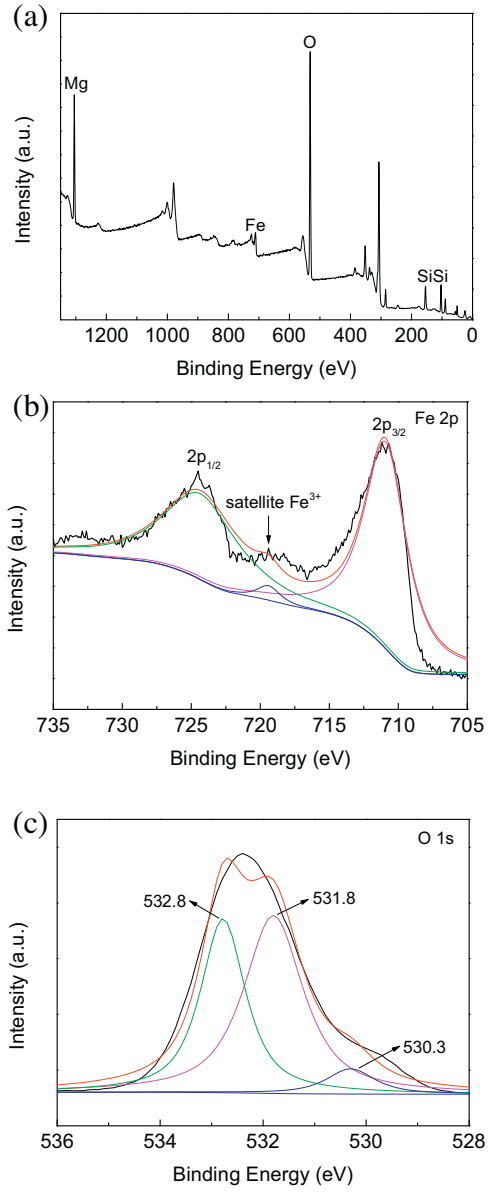

Fig. 3. XPS spectra of K-Fe: (a) the survey spectrum; (b) high-resolution Fe 2p; (c) high-resolution O1s.

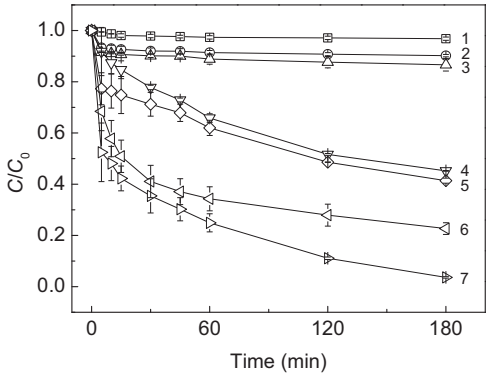

Fig. 4. Comparative study of RhB decolorization using: (1) Vis light, (2) K-Fe/dark, (3) K-Fe/Vis, (4) PS/dark, (5) K-Fe/PS/dark, (6) PS/Vis, and (7) K-Fe/PS/Vis. Reaction conditions: RhB (0.1 mM); K-Fe (0.4 g L^{-1}); PS (7.0 mM); initial pH 5.0.

reaction for 180 min in the dark (curve 4), thereby indicating that PS can directly react with RhB. Similarly with 7.0 mM PS, little or no enhancement of RhB decolorization in the dark was observed with K-Fe (curve 5), suggesting that PS cannot be activated by K-Fe in the absence of visible light irradiation. With PS alone, under irradiation with visible light, the decolorization efficiency of RhB was increased to 77% (curve 6) compared to that of 55% for PS in the dark. However, in the presence of both K-Fe and PS, the decolorization efficiency of RhB was considerably enhanced under visible light irradiation, and RhB was virtually completely decolorized (decolorization efficiency of 97%) within 180 min (curve 7). As stated above, the bleaching of RhB by PS can take place whether in the absence or presence of visible light irradiation and this is supported by the change of UV–Vis absorption spectra of the solution during the course of RhB decolorization (shown in Fig. S3), though, it was not completely decolorized after 180 min of irradiation.

The decolorization of RhB approximately followed pseudo-first-order kinetics (shown in the inset of Fig. S4). The kinetic enhancement of RhB decolorization over K-Fe is more significant in the presence of both PS and visible light irradiation (Fig. S4). The apparent rate constants of the processes of K-Fe/PS/Vis, PS/Vis and K-Fe/PS/dark are 1.57×10^{-2}, 6.60×10^{-3} and 4.10×10^{-3} min^{-1}, respectively. It is worthwhile noting that the apparent rate constant presented by the results of the K-Fe/PS/Vis process is much higher than the sum of the apparent rate constants presented by the results in the PS/Vis and K-Fe/PS/dark processes. This suggests that the synergistic effect of the K-Fe catalyst, PS and visible light illumination in the catalytic process could contribute cooperatively to the decolorization of RhB. Moreover, the synergistic effect in the K-Fe/PS/Vis process was quantitatively evaluated by using the synergistic index (SI): $SI = k_{KPV}/(k_{PV} + k_{KP})$, where k_{KPV}, k_{PV} and k_{KP} are the apparent rate constants presented by the results in the K-Fe/PS/Vis, PS/Vis and K-Fe/PS/dark processes, respectively. The value of the SI was calculated to be 1.47, indicating that the synergistic effect could enhance the catalytic activity of K-Fe by 47%.

3.3. Mechanistic insights

In order to understand the decolorization mechanism of RhB by the PS-based process, quenching experiments using ethyl alcohol (EtOH) as radical scavenger were firstly performed to check whether radicals were responsible for the observed decolorization. As shown in Fig. 5a, in the presence of EtOH (2.5 M), the decolorization of RhB in the PS/Vis process was significantly inhibited and a similar inhibition was observed when the catalyst was added to the process, indicating that radicals were involved with or without the addition of K-Fe. In addition, when 2.5 M EtOH was present in the PS/Vis process, the final degree of decolorization of RhB was quite close to that achieved in the PS/dark process, implying that the decolorization of RhB by PS alone was a non-radical process. To confirm this observation, EPR using 5,5-dimethyl-pyrroline-*N*-oxide (DMPO) as the radical trapping agent was employed to detect any radical formation. As can be seen from Fig. 5b, no signals of significant intensity were observed in the PS/dark process, confirming that the decolorization of RhB by PS alone resulted from a non-radical reaction. This phenomenon might be explained by the interaction between the RhB molecule and $S_2O_8^{2-}$ ion, where an electron transfer from RhB to PS occurred, subsequently resulting in the bleaching of the dye. With the addition of K-Fe, the EPR results were similar to those for PS alone in the dark, thus indicating that K-Fe was unable to activate PS if not irradiated. In contrast, when irradiated with visible light, signals for both DMPO-SO_4 and DMPO-OH adducts appeared in the PS/Vis process and these signals were enhanced by adding K-Fe (to produce the K-Fe/PS/Vis process), indicating more radicals were formed. These results provided evidence that irradiation with visible light could induce the

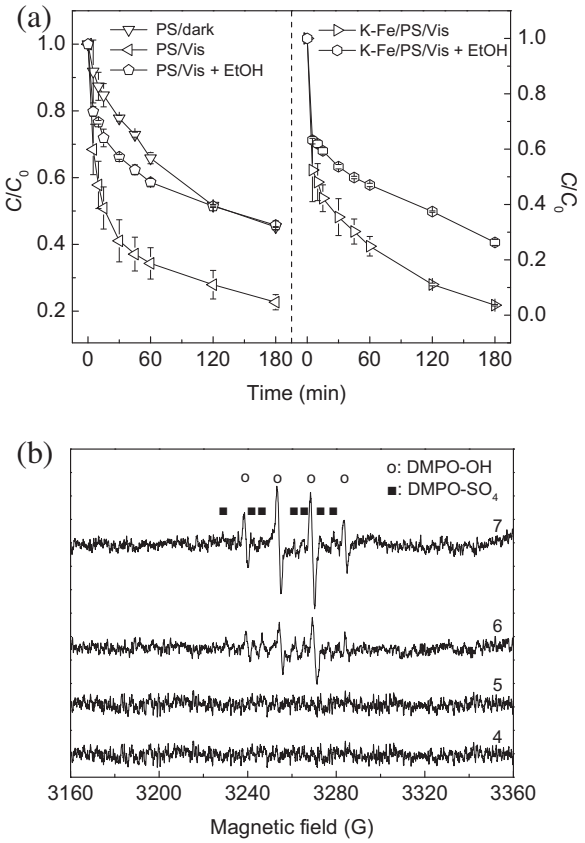

Fig. 5. (a) Effect of ethyl alcohol on the decolorization of RhB. Reaction conditions: RhB (0.1 mM); K-Fe (0.4 g L^{-1}), PS (7.0 mM); ethyl alcohol (2.5 M), initial pH 5.0. (b) EPR spectra in the processes of (4) PS/dark, (5) K-Fe/PS/dark, (6) PS/Vis and (7) K-Fe/PS/Vis. Reaction conditions: RhB (0.1 mM); PS (7.0 mM); DMPO (18 mM); initial pH 5.0; reaction time 15 min.

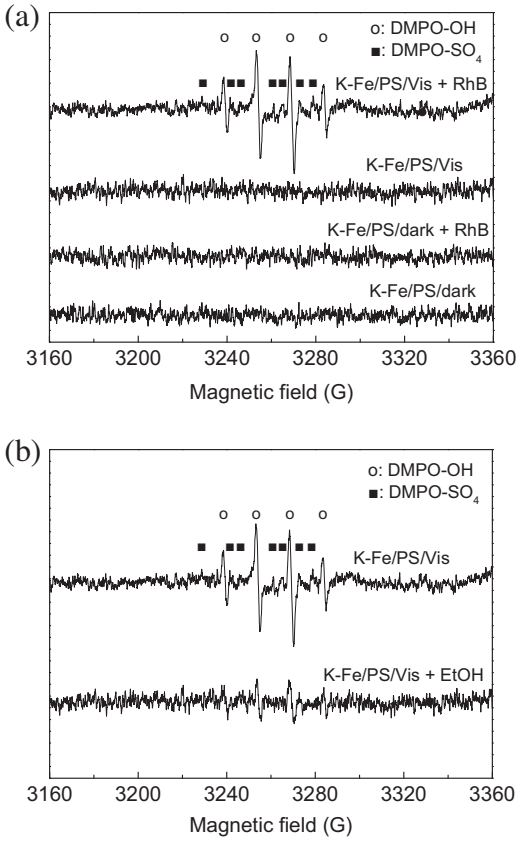

Fig. 6. (a) EPR spectra of various processes with and without RhB. Reaction conditions: RhB (0.1 mM); K-Fe (0.4 g L^{-1}); PS (7.0 mM); DMPO (18 mM); initial pH 5.0; reaction time 15 min. (b) EPR spectra of the K-Fe/PS/Vis process with and without ethyl alcohol. Reaction conditions: RhB (0.1 mM); K-Fe (0.4 g L^{-1}); PS (7.0 mM); DMPO (18 mM); ethyl alcohol (2.5 M); initial pH 5.0; reaction time 15 min.

generation of $SO_4^{\bullet-}$ and •OH radicals [34], and hence enhance the decolorization of RhB. It is well-known that the RhB molecule can absorb visible light, to produce the excited state of the dye [35] and the enhancement of removal of RhB under visible light irradiation is illustrated by equations (1-6) (the symbol ≡represents the iron species on the catalyst):

$$RhB + visiblelight \rightarrow RhB^* \quad (1)$$

$$RhB^* + S_2O_8^{2-} \rightarrow RhB^{+\bullet} + SO_4^{\bullet-}{}_{free} + SO_4^{2-} \quad (2)$$

$$RhB^* + \equiv Fe(III) \rightarrow \equiv Fe(II) + RhB^{+\bullet} \quad (3)$$

$$\equiv Fe(II) + S_2O_8^{2-} \rightarrow \equiv Fe(III) + SO_4^{\bullet-}adsorbed + SO_4^{2-} \quad (4)$$

$$SO_4^{\bullet-}{}_{free} + H_2O \rightarrow SO_4^{2-} + {}^{\bullet}OH_{free} + H^+ \quad (5)$$

$$SO_4^{\bullet-}adsorbed + free/{}^{\bullet}OH_{free} + RhB \rightarrow intermediates \quad (6)$$

To further confirm the photosensitization process induced by the dye upon visible light irradiation, further EPR experiments were performed and the results are illustrated in Fig. 6a. Without visible light irradiation, no characteristic peaks of DMPO spin adducts were detected whether the dye substrate was added or not. Similarly, no signals were detected in the irradiated suspension of K-Fe and PS in the absence of RhB. When exposed to visible light, however, both DMPO-SO_4 and DMPO-OH signals were detectable in the presence of RhB, indicating both $SO_4^{\bullet-}$ and •OH radicals were formed in the K-Fe/PS/Vis process [34]. This means that both RhB and visible light together are essential for the generation of both $SO_4^{\bullet-}$ and •OH radical species. Experiments were also performed by replacing RhB with phenol under identical conditions, since colorless phenol does not absorb visible light. The result, shown in Fig. S5, demonstrates that no significant absorbance change took place after 180 min of irradiation, indicating the dye-sensitization was a key factor in the reaction mechanism. Hence, it can be concluded that the decolorization of RhB over K-Fe in the presence of both PS and visible light irradiation is mainly due to the photosensitization of the dye itself.

Although both $SO_4^{\bullet-}$ and •OH radicals are involved in the PS-mediated photocatalytic process, an interesting phenomenon was observed when 2.5 M EtOH was added to the reaction. As previously depicted in Fig. 5a, in the presence of EtOH, the decolorization of RhB was inhibited by approximately 23% in the PS/Vis process. After the addition of K-Fe, the extent of inhibition of decolorization of RhB by EtOH in the K-Fe/PS/Vis process was also found to be about 23%, which was the same as that of the PS/Vis process. This seemed inconsistent with the EPR results obtained from Fig. 5b where more radicals appeared to be generated in the K-Fe/PS/Vis process compared to the PS/Vis process. To account for this surprising observation it should be noted that, besides the free radicals generated from activation of PS by RhB^*, surface-adsorbed radicals are also formed during the decolorization of RhB in the K-Fe/PS/Vis process. In order to further verify the existence of surface-adsorbed radicals, EPR experiments were conducted in the presence of EtOH. As illustrated in Fig. 6b, after the addition of 2.5 M EtOH, the intensity of the DMPO adducts decrease but the EPR signals are still observed, indicating that EtOH failed to trap the radicals formed on the surface of the catalyst, and confirmed the existence of such radicals during the decolorization of RhB in the K-Fe/PS/Vis process [36].

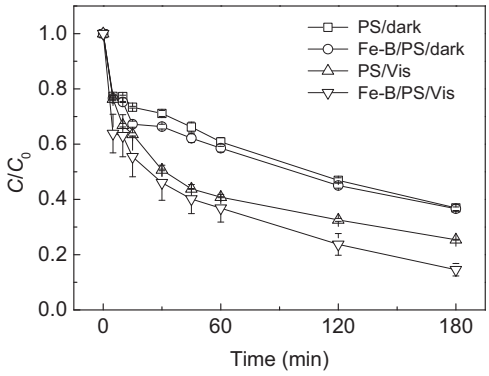

Fig. 7. Decolorization of RhB in various processes. Reaction conditions: RhB (0.2 mM); Fe-B (0.4 g L^{-1}); PS (3.5 mM); initial pH 5.0.

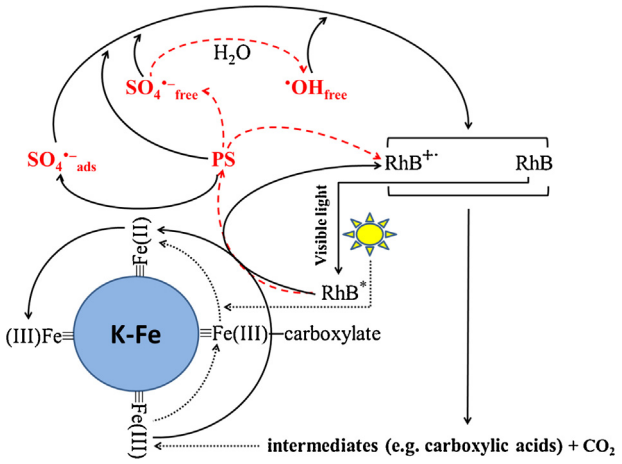

Fig. 8. Proposed mechanism of persulfate activation and RhB degradation in the K-Fe/PS/Vis process.

To assess the potential applicability of clay-based catalyst activated persulfate process for decontamination of organic pollutants in the presence of visible light irradiation, a different iron-supported clay catalyst using bentonite as support was synthesized (denoted as Fe-B [26]) using the same procedure for K-Fe and employed in the PS-based catalytic process. Considering that the Fe-B catalyst showed excellent adsorption performance toward the dye, the RhB concentration after adsorption equilibration was measured as the initial concentration (C_0). As shown in Fig. 7, the catalytic behavior of Fe-B for the photo-bleaching of RhB was similar to that of K-Fe indicating that the mechanism was similar for K-Fe and Fe-B. As mentioned above, the enhanced decolorization of RhB in the K-Fe/PS/Vis process was due to the synergistic effect of K-Fe, PS and visible light irradiation. However, the SI value for the Fe-B/PS/Vis process was found to be 1.04 according to the apparent rate constants shown in Fig. S6, revealing that the combination of Fe-B and PS under visible light irradiation exhibited only a slight synergistic effect in the decolorization of RhB.

Based on the findings above, a proposed mechanism for the decolorization of RhB using the K-Fe/PS/Vis process is depicted in Fig. 8. Under visible LED light irradiation, electron transfer and reduction of iron species are involved. RhB can absorb visible light and is promoted from the ground state to the excited state (Eq. (1)). Subsequently, the RhB^* can transfer electrons (i) to the $S_2O_8^{2-}$ ions to produce free $SO_4^{\bullet-}$ radicals and (ii) to ≡Fe(III) species to generate ≡Fe(II) species, as noted in Eqs. (2) and (3). The generated ≡Fe(II) species can also activate PS to yield surface-adsorbed $SO_4^{\bullet-}$ radicals (Eq. (4)). The produced free $SO_4^{\bullet-}$ radicals can convert to free

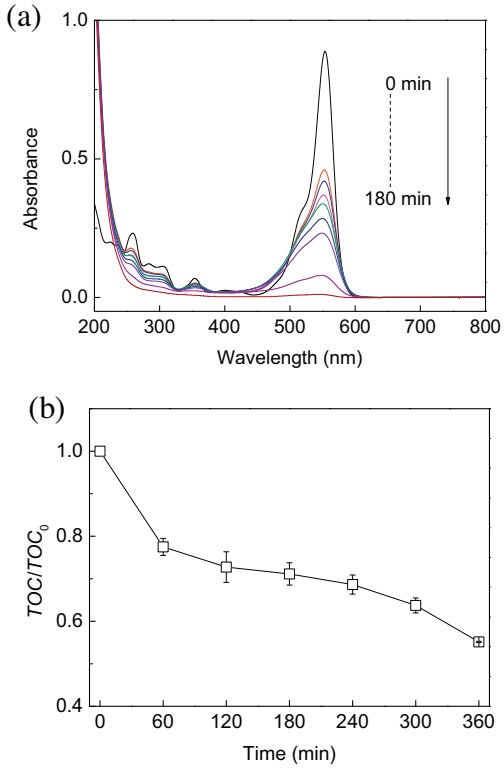

Fig. 9. (a) UV–Vis spectral changes with irradiation time and (b) the decrease of TOC in solution as a function of irradiation time. Reaction conditions: RhB (0.1 mM); K-Fe (0.4 g L^{-1}); PS (7.0 mM); initial pH 5.0.

•OH radicals through Eq. (5) [37]. Thereafter, the free and surface-adsorbed radicals produce decolorization of RhB in the K-Fe/PS/Vis process.

As previously shown in Fig. 4, the decolorization rates of the irradiated processes were much higher than of those in the dark, for example, K-Fe/PS/Vis > K-Fe/PS/dark, and PS/Vis > PS/dark. This indicated that electron transfer from the RhB^* to Fe(III) and PS played an important role in the decolorization of RhB. Therefore, the decolorization rate was higher within the first 60 min of irradiation in the K-Fe/PS/Vis process, due to the fact that more RhB molecules could be excited upon visible light irradiation. In the 60–180 min range, the decolorization rate became much slower since 75% of the RhB had been decolorized during the initial time period of 60 min, and the number of remaining RhB molecules, which could be excited to initiate the reaction, was significantly decreased. After the complete decolorization of RhB within 180 min, the electron transfer from the RhB^* to Fe(III) and PS ceased, however, the mineralization process in terms of TOC removal continued with the extension of irradiation time. This is probably an unexpected outcome of the photosensitization process and is discussed in detail below.

3.4. Changes in UV/Vis spectra and TOC measurements

Usually, the photocatalytic degradation of RhB occurs via two competitive processes: (i) *N*-de-ethylation and destruction of the conjugated structure and (ii) a hypsochromic shift of the absorption band presumed to be as a result of the formation of a series of *N*-de-ethylated intermediates in a stepwise manner [38,39]. However, no evident absorption band shift was observed in the K-Fe/PS/Vis process, implying the destruction of the conjugated xanthene ring in RhB (see Fig. S7 for molecular structure of RhB) [39,40]. From Fig. 9a, it is seen that both the main absorbance in the visible region and

the peaks in the UV region are decreased on irradiation, indicating that the dye chromophores and the aromatic ring are destroyed, meaning that RhB was not only decolorized but also degraded [40].

To provide further evidence that RhB had been degraded during oxidation, the extent of mineralization of RhB was determined during the K-Fe/PS/Vis process. Fig. 9b clearly shows that in the initial time period of 60 min, approximately 22% TOC removal was observed and this could be attributed to the adsorption of the dye from aqueous solution and the positive influence of the presence of PS [41,42]. In order to identify the contribution of adsorption to the initial TOC removal, the fresh K-Fe, the used K-Fe after 60 min of reaction, and the used K-Fe after 360 min of reaction were examined using FTIR spectroscopy. Compared to fresh K-Fe, the FTIR spectrum of the used K-Fe after 60 min showed the characteristic absorption peaks of the dye in the fingerprint region (the red dotted box in Fig. S8). Nevertheless, these characteristic peaks all disappeared in the used K-Fe after 360 min, indicating that adsorption made a contribution to the initial TOC removal. On the other hand, in the presence of PS, the solution pH decreased during the course of the reaction due to formation of hydrogen ions according to Reaction (5). As can be seen from Table S1, the decrease of pH was most significant within the first 60 min of irradiation, which positively influenced the mineralization rate but thereafter, the TOC removal was slower though a decrease of nearly 45% in TOC was achieved over 360 min. However, for the mineralization of RhB in the K-Fe/PS/Vis process, the trend of TOC removal was totally different from that previously reported for the Vis/TiO_2/PMS process [43]. In the latter process once the reaction was decolorized, there were no species present that could be excited by visible light irradiation, and thus the mineralization process ceased. However, in the current process, a further decrease in TOC of approximately 13% was noted even after complete decolorization of RhB (180 min of irradiation). This might be due to the formation of some degradation products, such as oxalic acid, which could complex with ≡Fe(III) to form ≡Fe(III)–carboxylate which could behave as photochemically active compounds in the UV–Vis range of 250–480 nm and undergo a photochemical reaction to yield ≡Fe(II) [44,45]. To confirm the generation of any ≡Fe(II) species, the high resolution XPS spectrum for Fe2p regions of the used K-Fe after 360 min was examined (Fig. S9) and the appearance of a new peak at 710.6 eV was observed, indicating the presence of Fe(II) [36]. Interestingly, the proportion of Fe(II) was found to be 12%, confirming that Fe(II) species could be formed even after the RhB was completely decolorized. The resulting ≡Fe(II) species could then react with PS to produce the $SO_4^{\bullet-}$ radical, as indirectly evidenced by the experimental fact that a further decomposition in PS of approximately 14% was noted by prolonging the irradiation time from 180 to 360 min. Thus, the resultant surface-bound radical species accounts for the improvement in TOC removal after the complete decolorization of RhB.

3.5. Reusability of K-Fe

From an economic perspective, reusability is an important factor for the successful application of a good heterogeneous catalyst in a solid–liquid reaction. Five consecutive experiments were carried out to examine the retention of photocatalytic ability of the K-Fe. As illustrated in Fig. 10, no discernible change in the photocatalytic activity of the recycled catalyst was noticed after each run, indicating that K-Fe could be used for sustainable photocatalytic oxidation processes in the presence of visible light illumination.

3.6. Effect of several parameters on the photocatalytic degradation of RhB

The amount of catalyst, the oxidant concentration and the initial pH can significantly influence the catalytic reaction so the effects

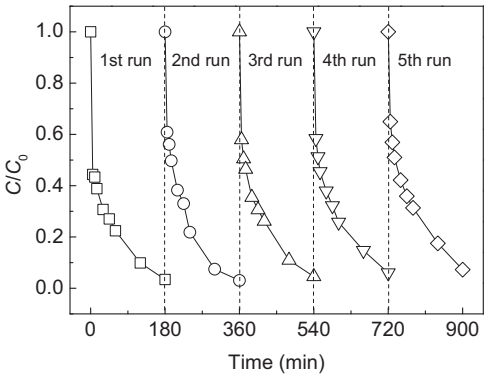

Fig. 10. The reusability of K-Fe for the photocatalytic degradation of RhB mediated by persulfate under visible LED light irradiation. Reaction conditions: RhB (0.1 mM); K-Fe (0.4 g L^{-1}); PS (7.0 mM); initial pH 5.0.

of these three factors on the degradation of RhB by K-Fe in the PS-mediated photocatalytic process were assessed. When the K-Fe dosage is raised from 0.1 to 0.4 g L^{-1}, the degradation of RhB is slightly accelerated, mainly due to the increase in the active sites for decomposing PS to generate more radicals (Fig. 11a). However, the amount of degradation was not increased, but rather declined a little, when the K-Fe dosage was increased to 0.8 g L^{-1}, probably due to the obstruction of visible light pathway by the suspended solid particles at the higher concentration [24] and these two distinct effects could reach a balance at the optimal catalyst dosage of 0.4 g L^{-1} [31].

As shown in Fig. 11b, an increase in the PS concentration in the range of 1.0 to 7.0 mM led to a significant enhancement in the extent of degradation from 66% to 97%, because more radicals had been formed. Nevertheless, at the highest dosage of PS (i.e., 10.5 mM), no pronounced additional enhancement was noticed owing to the occurrence of scavenging reactions, as expressed by the following equations [10]:

$$SO_4^{\bullet-} + S_2O_8^{2-} \rightarrow S_2O_8^{-\bullet} + SO_4^{2-} \quad (7)$$

$$2SO_4^{\bullet-} \rightarrow S_2O_8^{2-} \quad (8)$$

Therefore, the optimal concentration of PS should be just sufficient to be converted into the $SO_4^{\bullet-}$ radical required to oxidize RhB but scavenging of the $SO_4^{\bullet-}$ radical must be avoided [46]. In the K-Fe/PS/Vis process, the optimal concentration of initial PS was 7.0 mM, which is close to 7.3 mM calculated according to the theoretical stoichiometry for the complete mineralization of 0.1 mM RhB by PS (Eq. (9)).

$$C_{28}H_{31}ClN_2O_3 + 73\,S_2O_8^{2-} + 59\,H_2O \rightarrow 28CO_2 + 149\,H^+ + Cl^- + 2NO_3^- + 146SO_4^{2-} \quad (9)$$

The solution pH is known to be one of the decisive factors affecting not only the catalytic reaction but also the extent of iron leaching from the solid catalyst (and thus the stability of the catalyst). Fig. 11c shows the effect of initial pH on the degradation of RhB and it can be seen that activation of PS by K-Fe under visible light irradiation was effective over a wider pH range (from 3.0 to 9.0) for the degradation of RhB, compared to the narrow pH range of 2.0–4.0 for conventional homogeneous Fenton-like processes [47]. With the normal pH of 5.0 for 0.1 mM RhB solution, excellent degradation efficiency was achieved, indicating that the photocatalytic degradation of RhB could be performed at near-neutral pH without any pH pre-adjustment. With reference to the long-term stability of the catalyst, the iron leaching from K-Fe at different solution pH was monitored and the results displayed in Fig. S10. The concentration of iron leached from the catalyst into the aqueous phase, in

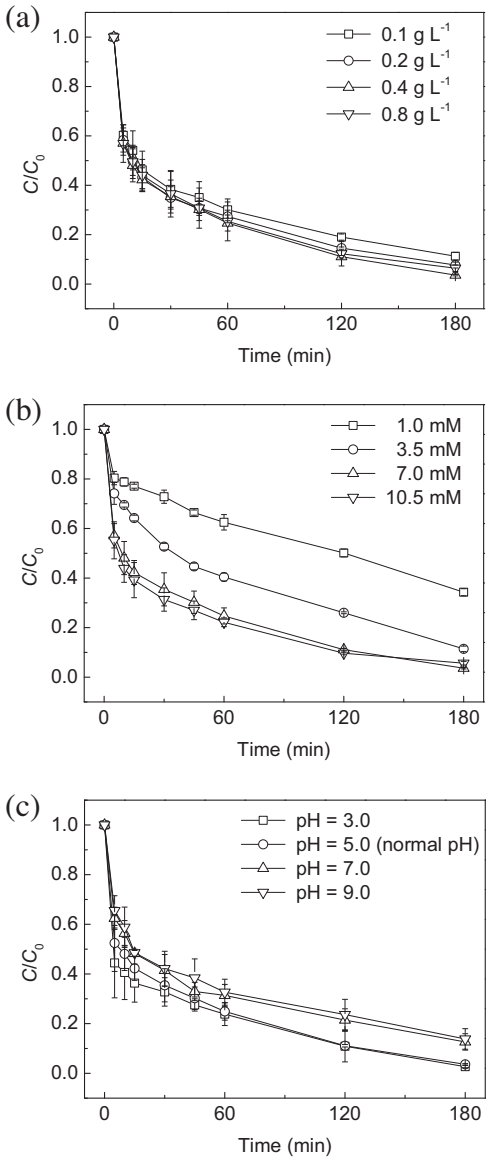

Fig. 11. Effects of several parameters on the photocatalytic degradation of RhB in the K-Fe/PS/Vis process: (a) catalyst concentration; (b) amount of PS; (c) initial pH. Reaction conditions: (a) RhB (0.1 mM); PS (7.0 mM); initial pH 5.0; (b) RhB (0.1 mM); K-Fe (0.4 g L^{-1}); initial pH 5.0; (c) RhB (0.1 mM); K-Fe (0.4 g L^{-1}); PS (7.0 mM).

the worst case (i.e., pH 3.0) was below 0.5 mg L^{-1}, which is considered negligible from the catalytic perspective, suggesting that the K-Fe is quite stable and the observed photocatalytic process was intrinsically heterogeneous.

4. Conclusions

An inexpensive clay/iron-based catalyst was prepared and used for the first time for the photocatalytic degradation of an organic dye in aqueous media through activation of persulfate under visible LED irradiation. In the K-Fe/PS/Vis process, persulfate degrades RhB via an electron transfer pathway where the excitation of RhB by visible light irradiation (i) activates persulfate which then generates free radicals and (ii) promotes the cycling of ≡Fe(II) and ≡Fe(III) species. The results of quenching experiments and EPR studies indicated that the free radicals formed from persulfate by RhB^*, along with the surface-adsorbed radicals resulting from the reaction between persulfate and ≡Fe(II) species on the catalyst were responsible for the photocatalytic degradation of RhB. The present study elucidated a new pathway of persulfate activation resulting in efficient phtocatalytic degradation of RhB over a wide pH range, and which may provide useful information for the treatment of dye-containing wastewater. In order to further define the degradation pathway future work will focus on the identification of degradation intermediates.

Acknowledgements

This work was supported by Natural Science Foundation of Hubei Province(Grant No. 2012FFA089), Natural Science Foundation of China(Grant No. 21547006) and Shenzhen Basic Research Plan Project(Grant No. JCYJ20150508152951667). The analyses of FESEM, EDS, XRD and XPS were partially supported by Large-scale Instrument and Equipment Sharing Foundation of Wuhan University. The generous help of Professor David H. Bremner in revising this manuscript is greatly appreciated.

Appendix A. Supplementary data

Supplementary data associated with this article can be found, in the online version, at http://dx.doi.org/10.1016/j.apcatb.2015.12.002.

References

[1] Y. Yang, J.J. Pignatello, J. Ma, W.A. Mitch, Environ. Sci. Technol. 48 (2014) 2344–2351.
[2] M. Antonopoulou, E. Evgenidou, D. Lambropoulou, I. Konstantinou, Water Res. 53 (2014) 215–234.
[3] M.A. Oturan, J.J. Aaron, Crit. Rev. Environ. Sci. Technol. 44 (2014) 2577–2641.
[4] G.P. Anipsitakis, D.D. Dionysiou, Appl. Catal. B: Environ. 54 (2004) 155–163.
[5] Y.F. Huang, Y.H. Huang, J. Hazard. Mater. 162 (2009) 1211–1216.
[6] G. Fang, J. Gao, D.D. Dionysiou, C. Liu, D. Zhou, Environ. Sci. Technol. 47 (2013) 4605–4611.
[7] M.M. Ahmed, S. Chiron, Water Res. 48 (2014) 229–236.
[8] C. Cai, H. Zhang, X. Zhong, L. Hou, Water Res. 66 (2014) 473–485.
[9] H. Sun, S. Liu, S. Liu, S. Wang, Appl. Catal. B: Environ. 146 (2014) 162–168.
[10] P. Avetta, A. Pensato, M. Minella, M. Malandrino, V. Maurino, C. Minero, K. Hanna, D. Vione, Environ. Sci. Technol. 49 (2015) 1043–1050.
[11] C. Tan, N. Gao, Y. Deng, N. An, J. Deng, Chem. Eng. J. 203 (2012) 294–300.
[12] M. Mahdi-Ahmed, S. Chiron, J. Hazard. Mater. 265 (2014) 41–46.
[13] G.P. Anipsitakis, D.D. Dionysiou, Environ. Sci. Technol. 38 (2004) 3705–3712.
[14] C. Liang, C.J. Bruell, M.C. Marley, K.L. Sperry, Chemosphere 55 (2004) 1213–1223.
[15] X.R. Xu, X.Z. Li, Sep. Purif. Technol. 72 (2010) 105–111.
[16] S. Rodriguez, L. Vasquez, D. Costa, A. Romero, A. Santos, Chemosphere 101 (2014) 86–92.
[17] S. Navalon, M. Alvaro, H. Garcia, Appl. Catal. B: Environ. 99 (2010) 1–26.
[18] J. Herney-Ramirez, M.A. Vicente, L.M. Madeira, Appl. Catal. B: Environ. 98 (2010) 10–26.
[19] H. Lim, J. Lee, S. Jin, J. Kim, J. Yoon, T. Hyeon, Chem. Commun. 4 (2006) 463–465.
[20] R. Gonzalez-Olmos, F.D. Kopinke, K. Mackenzie, A. Georgi, Environ. Sci. Technol. 47 (2013) 2353–2360.
[21] F. Gong, L. Wang, D. Li, F. Zhou, Y. Yao, W. Lu, S. Huang, W. Chen, Chem. Eng. J. 267 (2015) 102–110.
[22] M. Luo, D. Bowden, P. Brimblecombe, Appl. Catal. B: Environ. 85 (2009) 201–206.
[23] G. Zhang, Y. Gao, Y. Zhang, Y. Guo, Environ. Sci. Technol. 44 (2010) 6384–6389.
[24] X. Zhao, L. Zhu, Y. Zhang, J. Yan, X. Lu, Y. Huang, H. Tang, J. Hazard. Mater. 215-216 (2012) 57–64.
[25] A.N. Soon, B. Hameed, Desalination 269 (2011) 1–16.
[26] Y. Gao, Y. Wang, H. Zhang, Appl. Catal. B: Environ. 178 (2015) 29–36.
[27] W.K. Jo, R.J. Tayade, Ind. Eng. Chem. Res. 53 (2014) 2073–2084.
[28] X. Wang, T.T. Lim, Appl. Catal. B: Environ. 100 (2010) 355–364.
[29] S. Guo, G. Zhang, J. Wang, J. Colloid Interf. Sci. 433 (2014) 1–8.
[30] X. Zhang, S. Lin, Z. Chen, M. Megharaj, R. Naidu, Water Res. 45 (2011) 3481–3488.
[31] Y. Wang, Y. Sun, W. Li, W. Tian, A. Irini, Chem. Eng. J. 267 (2015) 1–8.
[32] S. Wang, L. Wang, T. Yang, X. Liu, J. Zhang, B. Zhu, S. Zhang, W. Huang, S. Wu, J. Solid State Chem. 183 (2010) 2869–2876.
[33] H. Ma, B. Wang, Y. Wang, J. Hazard. Mater. 145 (2007) 417–423.
[34] C. Tan, N. Gao, Y. Deng, J. Deng, S. Zhou, J. Li, X. Xin, J. Hazard. Mater. 276 (2014) 452–460.
[35] H. Fu, C. Pan, W. Yao, Y. Zhu, J. Phys. Chem. B 109 (2005) 22432–22439.

[36] Y. Lei, C.S. Chen, Y.J. Tu, Y.H. Huang, H. Zhang, Environ. Sci. Technol. 49 (2015) 6838–6845.
[37] C. Liang, Z.S. Wang, C.J. Bruell, Chemosphere 66 (2007) 106–113.
[38] C. Chen, W. Zhao, J. Li, J. Zhao, Environ. Sci. Technol. 36 (2002) 3604–3611.
[39] P. Lei, C. Chen, J. Yang, W. Ma, J. Zhao, L. Zang, Environ. Sci. Technol. 39 (2005) 8466–8474.
[40] M. Yin, Z. Li, J. Kou, Z. Zou, Environ. Sci. Technol. 43 (2009) 8361–8366.
[41] R. Vinu, S. Polisetti, G. Madras, Chem. Eng. J. 165 (2010) 784–797.
[42] V. Augugliaro, C. Baiocchi, A.B. Prevot, E. Garcia-Lopze, V. Loddo, S. Malato, G. Marci, L. Palmisano, M. Pazzi, E. Pramauro, Chemosphere 49 (2002) 1223–1230.
[43] X. Chen, W. Wang, H. Xiao, C. Hong, F. Zhu, Y. Yao, Z. Xue, Chem. Eng. J. 193-194 (2012) 290–295.
[44] Y. Wang, R. Priambodo, H. Zhang, Y.H. Huang, RSC Adv. 5 (2015) 45276–45283.
[45] V. Kavitha, K. Palanivelu, J. Photochem. Photobiol. A: Chem. 170 (2005) 83–95.
[46] R. Su, J. Sun, Y. Sun, K. Deng, D. Cha, D. Wang, Chemosphere 77 (2009) 1146–1151.
[47] J. Pignatello, E. Oliveros, A. Mackay, Crit. Rev. Environ. Sci. Technol. 36 (2006) 1–84.